Targeted Reactant Activation and Spatial Charge Separation for Efficient Photocatalytic C(sp^3)-H Bond Oxidation

Taoran Chen[1,2#], Yu Han[1,2#], Guojin Huang[1,2], Zhengwu Liao[1,2], Yulin Wang[1,2], Ying Tao[1,2], Yue Zheng[1,2], Yu Wang[1,2], Shiqi Li[3], Wei Zhao[3], Hongli Sun[1,2,*], Chenliang Su[1,2]

[1] International Collaboration Laboratory of 2D Materials for Optoelectronics Science and Technology of Ministry of Education, Institute of Microscale Optoelectronics, Shenzhen University, Shenzhen 518060, China

[2] State Key Laboratory of Radio Frequency Heterogeneous Integration, Shenzhen University, Shenzhen 518060, China

[3] Institute for Advanced Study, Shenzhen University, Shenzhen, 518060, China

**To whom correspondence should be addressed*

E-mail: hlsun@szu.edu.cn

1 Experimental section

1.1 Materials

Cesium bromide (CsBr, 99.5 %), cesium chloride (CsCl, 99 %), bismuth bromide ($BiBr_3$, 98 %), 5,5-dimethyl-1-pyrroline-N-oxide (DMPO), ethylbenzene, cyclohexane, toluene-d8, diphenylmethane, benzyl alcohol, and tetrabutylammonium hexafluorophosphate ($TBAPF_6$) were purchased from Macklin Inc. (Shanghai, China). Methanol (99.5 %) and $AgNO_3$ (99 %) were purchased from Energy chemical. Melamine (99 %) and 1,4-Benzoquinone (97 %) were purchased from Aladdin. N, N-Dimethylformamide (DMF), isopropanol, acetonitrile (CH_3CN), ethyl acetate and toluene were obtained from Sinopharm Chemical Reagent Co., Ltd. (Shanghai, China). O_2 and Ar were purchased from Shenzhen Huatepeng SPECIAL Gases Co., Ltd.

1.2 Sample preparation

Preparation of CsPCN: Firstly, weigh melamine and CsCl in mortar, then the mixture was ground for 1 hour to achieve homogeneity. Subsequently, the mixture was spread evenly in a crucible and heated at a rate of 5 ℃·min^{-1} up to 550 ℃, holding the temperature constant for 4 hours. After the reaction, the furnace was cooled naturally to room temperature. Finally, the resulting product was collected as a pale-yellow powder, which was designated as CsPCN.

Synthesis of $Cs_3Bi_2Br_9$: $Cs_3Bi_2Br_9$ (CBB) was prepared by a well-established anti-solvent precipitation method at room temperature. Specifically, 3 mmol of CsBr, and 2 mmol of $BiBr_3$ were added into 50 mL of N, N-Dimethylformamide (DMF) by ultrasonication. Then, the mixture was added into 80 mL ethyl acetate under vigorous stirring, which generated precipitation. After that, the precipitation was centrifuged at 10000 rpm for 5 minutes, washed with ethyl acetate for 3 times, then dried in a vacuum oven at 60 °C for 12 h.

Synthesis of CsPCN-$Cs_3Bi_2Br_9$: CsPCN-$Cs_3Bi_2Br_9$ (CsPCN-CBB) was synthesized via the same procedure for the synthesis of $Cs_3Bi_2Br_9$ with the addition of CsPCN. In brief,

a certain amount of CsPCN (5, 15, 25, 35, 50 mg) was firstly dispersed in 50 mL of N, N-Dimethylformamide (DMF) by ultrasonication. Then, 3 mmol of CsBr, and 2 mmol of $BiBr_3$ were added into the solution. After fully dissolving of the CsBr and $BiBr_3$, the mixture was added dropwise into 80 mL ethyl acetate under vigorous stirring, which generated precipitation. After that, the precipitation was centrifuged, washed with ethyl acetate for 3 times, then dried in a vacuum oven at 60 °C for 12 h.

1.3 Characterizations

Scanning electron microscope (SEM) images of the samples were characterized by Hitachi 8100. Transmission electron microscopy (TEM) and high-resolution transmission electron microscopy (HRTEM) images were recorded using a JEOL JEM-F200 at an accelerating voltage of 100 kV. The X-ray diffraction (XRD) analysis with Cu Kα radiation (Rigaku Ultima IV) over a 2θ range of 5-80°. The scan rate was set at 5° per minute, employing a current of 40 mA and a voltage of 40 kV. The optical properties were investigated via UV-Vis-NIR spectroscopy using a Varian Cary 5000 Scan system (Agilent) using 100% $BaSO_4$ as an internal standard. X-ray photoelectron spectroscopy (XPS) and *in-situ* XPS was recorded on Empyrean (PANalytical) equipped with a monochromatic Al Kα as the X-ray source. All binding energies were referenced to the C 1s peak at 284.8 eV of surface adventitious carbon. Photoluminescence (PL) and time-resolved transient photoluminescence (TRPL) measurements were performed on a HORIBA Fluorolog-3 spectrofluorometer. Temperature-dependent Photoluminescence were performed on a spectrapro hrs-500. FT-IR and *in-situ* DRIFTS were performed on VERTEX 70v (Bruker). Electron paramagnetic resonance (EPR) spectrometer was used to characterize radicals in the reaction system. EPR spectra were measured on CIQTEK EPR 200 M with continues-wave X band frequency.

1.4 Electrochemical measurements

All the electrochemical measurements were using a three-electrode quartz cell with an electrochemical workstation (CHI 660E). A Pt plate and Ag/AgCl electrode were

employed as the counter electrode (CE) and reference electrode (RE), respectively. The working electrode was prepared on fluorine-doped tin oxide (FTO) glass that was cleaned with deionized water, absolute ethanol, respectively for 30 min. Typically, 5 mg of catalyst was dispersed in 0.1 mL of isopropanol to get slurry. After that, 50 μL of the slurry was spread on the conductive surface of the FTO glass and then dried at 60 °C for 2 h to improve adhesion. The exposed area of the working electrode was 1 cm^2. The electrochemical impedance spectroscopy (EIS) measurement was carried out in an electrolyte of 0.1 M $TBAPF_6$ containing acetonitrile solution in a frequency range from 0.1 Hz to 1 M Hz. The photocurrent measurement and open-circuit potential decay plots was performed under visible light irradiation using a 300 W Xenon lamp source (PLS-SXE 300D, Beijing Perfectlight Technology Co., Ltd.).

1.5 Temperature-dependent continuous photoluminescence spectroscopy

Temperature-dependent continuous photoluminescence (TD-PL) measurements were carried out on a Scan Pro Advance photoelectric testing system (Metatest Corporation). A pellet was prepared by compressing 100 mg of the sample. This pellet was placed in the measurement chamber, which was maintained under low pressure for 3 hours. Subsequently, liquid helium was introduced into the system. The photocatalyst was then excited at 370 nm, and its TD-PL spectra were recorded over a temperature range of 10-300 K using a 450 W xenon lamp.

1.6 *In-situ* DRIFTS measurements

In-situ diffuse reflectance infrared Fourier transform spectroscopy (*In-situ* DRIFTS) was employed to monitor the adsorption and photocatalytic transformation of ethylbenzene on the catalyst surface. Approximately 100 mg of catalyst was uniformly spread on the porous ceramic sample holder in the *in-situ* DRIFTS cell and gently pressed to obtain a flat, dense layer. Prior to each experiment, the sample was pretreated under a flow of high-purity O_2 to remove impurities, then cooled to room temperature under the same atmosphere. Ethylbenzene was introduced by passing an O_2 stream through liquid ethylbenzene and directing the resulting gas mixture over the catalyst

surface. The gas flow was maintained for 30 min in the dark until the characteristic vibrational bands of adsorbed ethylbenzene no longer increased in intensity, indicating that adsorption equilibrium (surface saturation) had been reached. The spectrum collected at this stage was taken as the reference state for the adsorbed reactant. Subsequently, the catalyst bed was irradiated with visible light 300 W Xenon lamp source (PLS-SXE 300D, Beijing Perfectlight Technology Co., Ltd.) under continuous O_2 flow, and *in-situ* DRIFTS spectra were recorded over 60 min at defined time intervals to track the evolution of surface species.

1.7 Electron paramagnetic resonance spectroscopy measurements

The EPR test for $\cdot CH_2Ph$ was conducted using 5,5 dimethyl-1-pyrroline-N-oxide (DMPO) as an indicator. Typically, 10 mg sample were dispersed in a mixed solution of 1 mL CH_3CN containing 20 μL ethylbenzene and 0.5 mM DMPO. Then, the suspension was transferred into a glass capillary, which was further placed in a glass tube under oxygen (O_2) atmosphere. After that, the glass tube was placed in the microwave cavity of EPR spectrometer and was irradiated by a 300 W Xenon lamp source at room temperature. The detection of superoxide radical was conducted using DMPO as a trapping agent. Similarly, 10 mg of sample was dispersed in a mixed solution of 0.5 mL of CH_3CN and 10 μL of DMPO. The suspension was transferred into a glass capillary, which was further placed inside a sealed glass tube. This tube was subsequently placed in the microwave cavity of the EPR spectrometer and irradiated by a 300 W Xe lamp source (PLS-SXE 300D, Beijing Perfect-light Technology Co., Ltd.) as the light source.

1.8 Photocatalytic measurements

The photocatalytic activity of the prepared catalysts was evaluated for oxidation of benzylic C(sp^3)-H bond in a quartz reactor. Initially, 5 mg of photocatalyst was added into 4 mL of CH_3CN and 1 mL ethylbenzene. The mixture was bubbled with O_2 gas for 10 min. Then, the reaction was proceeded under light irradiation from PCX-50C Discover (Beijing Perfect-light) irradiated by visible lamp (wavelength 400-800 nm).

After the reaction, the liquid products were analyzed using a gas chromatograph Fuli 9790 (Fuli, China, FID detector) after centrifugation at 10000 rpm for 3 minutes. The selectivity of products was detected by a gas chromatography-mass spectrometer (GC-MS) (Agilent 7820A, USA).

1.9 Apparent quantum yield measurement

The apparent quantum yield (AQY) of acetophenone formed on CsPCN-CBB were tested, which was obtained under the Xenon lamp equipped with single-wavelength filters (380, 420, 500, 600 nm). Depending on the amount of converted ethylbenzene by the photocatalytic reaction, the AQY was calculated as follow:

$$AQY = \frac{Ne}{Np} \times 100\% = \frac{n \times N_A \times h \times c}{P \times S \times t \times \lambda}$$

Where, *Ne* represents the number of electrons available for production of acetophenone, *Np* represents the number of incident photons, *n* represents the amount of acetophenone (umol), N_A is Avogadro constant (6.022×10^{23} mol^{-1}), h is the Planck constant (6.626×10^{-34} J·s), c is the light speed (3×10^{8} m s^{-1}), S represents the irradiation area (cm^2), P represents the intensity of irradiation light (W cm^{-2}), t is irradiation time(s), λ is the wavelength of monochromatic light (m).

2 Figures and tables

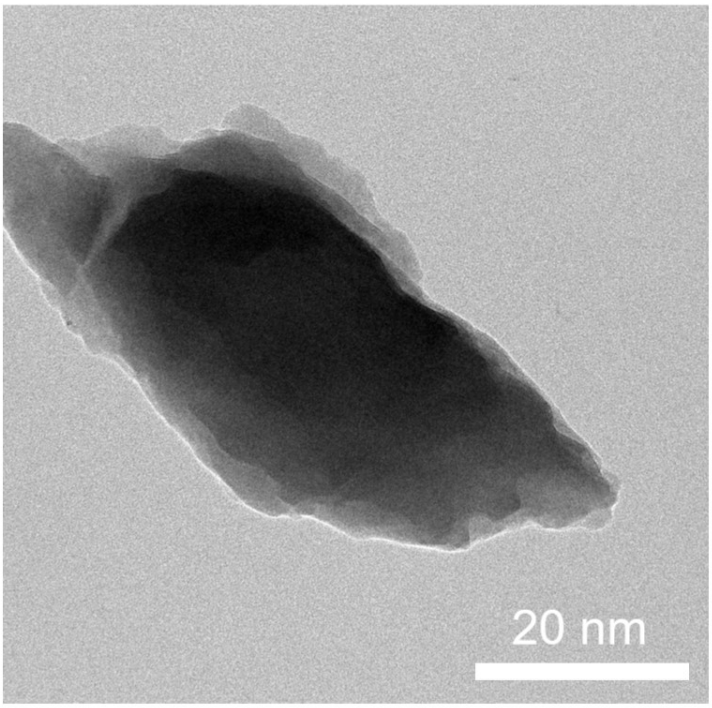

Figure S1. TEM image of blank CsPCN.

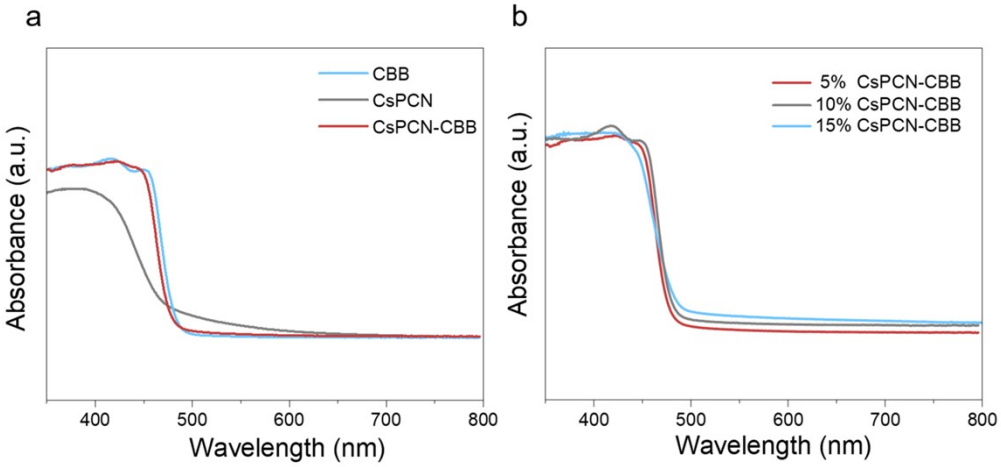

Figure S2. UV-Vis diffuse reflectance spectra of CBB, CsPCN and CsPCN-CBB.

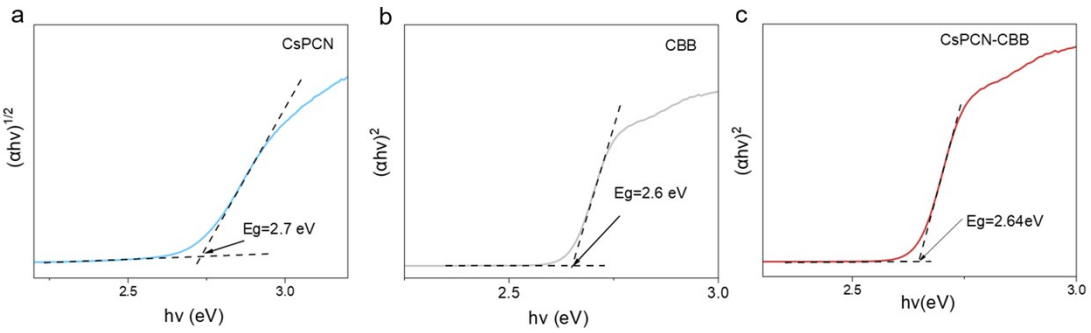

Figure S3. Tauc plots of (a) CsPCN, (b) CBB and (c) CsPCN-CBB composite.

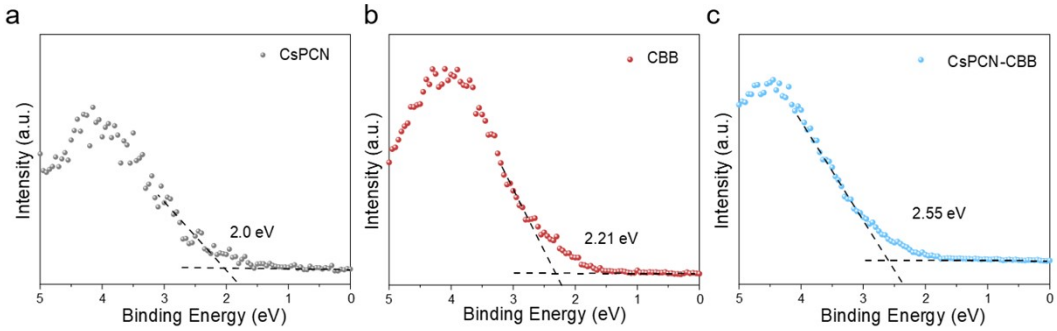

Figure S4. XPS valence band spectra of (a) CsPCN, (b) CBB and (c) CsPCN-CBB composite.

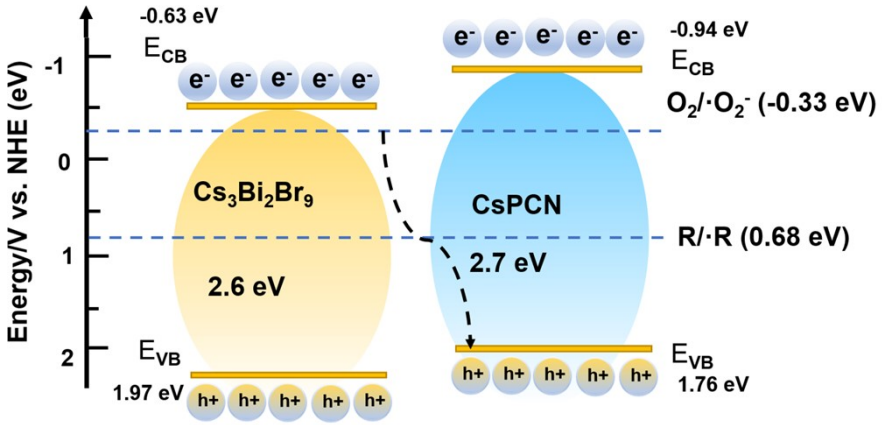

Figure S5. Band structure diagram and charge transfer mechanism of the CsPCN-CBB heterojunction.

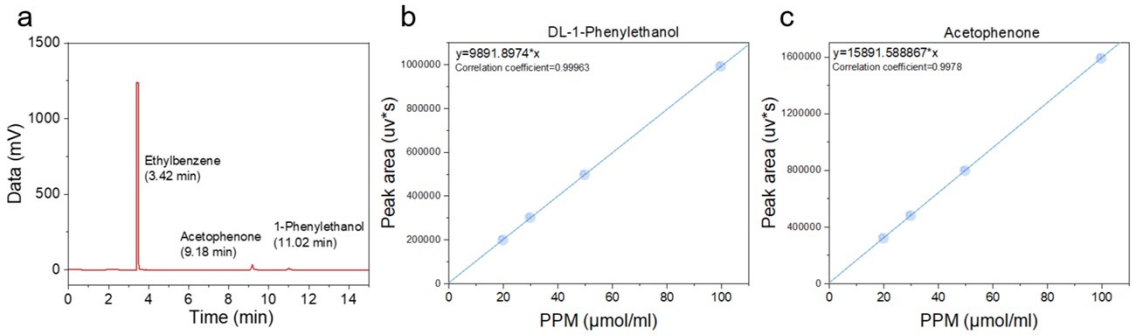

Figure S6. Standard curve of acetophenone and 1-Phenylethanol composite.

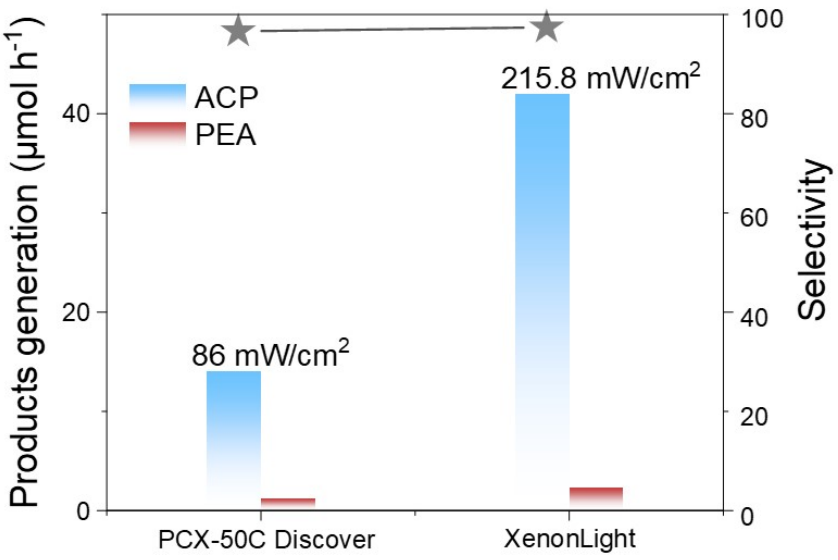

Figure S7. Photocatalytic performance under different light sources.

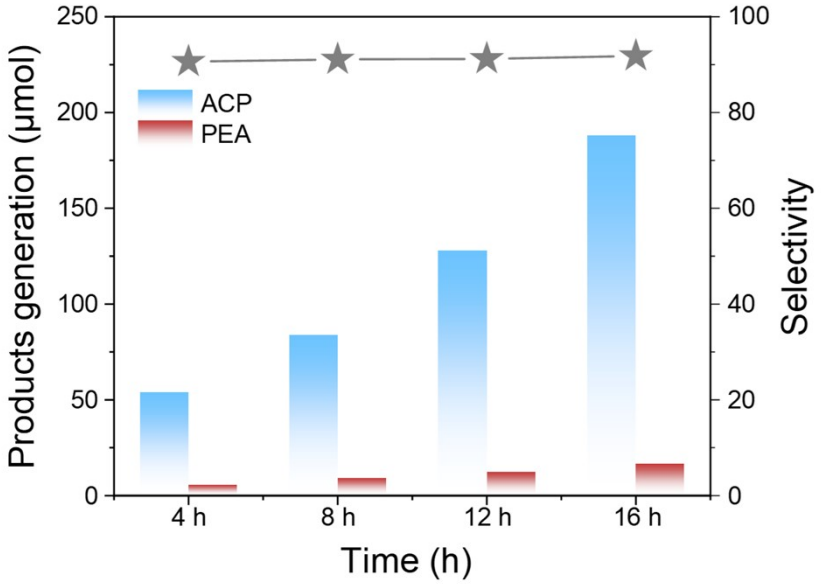

Figure S8. The long-time photoactivity over CsPCN-CBB composite.

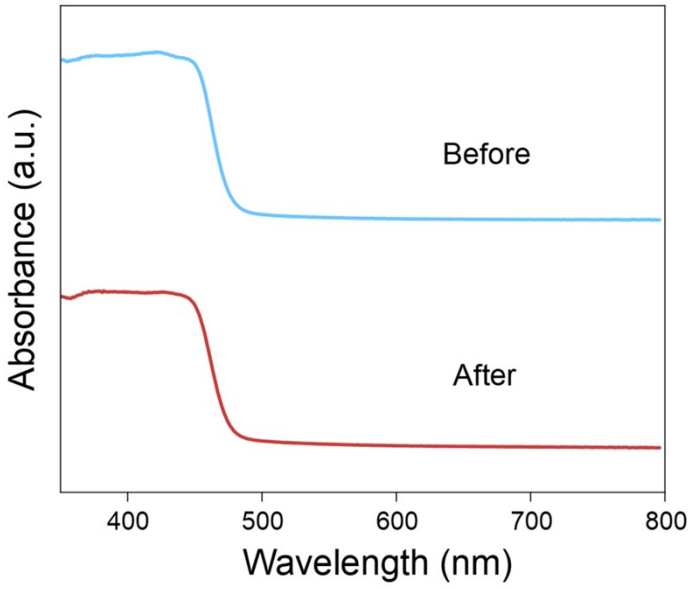

Figure S9. UV-vis DRS of CsPCN-CBB composite before and after the reaction.

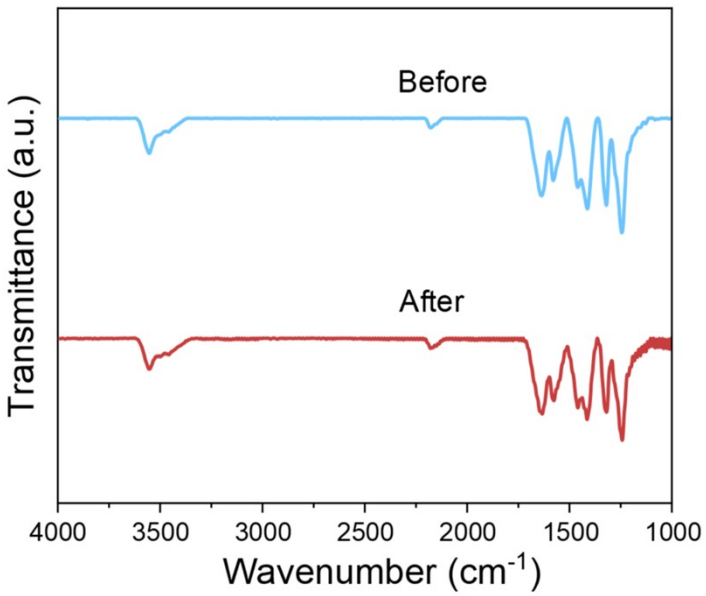

Figure S10. FT-IR of CsPCN-CBB composite before and after the long-time stability test.

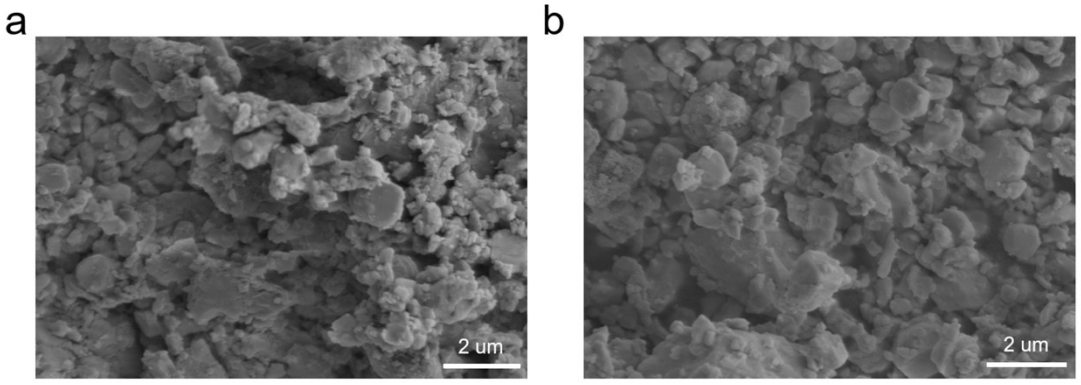

Figure S11. SEM images of CsPCN-CBB composite (a) before and (b) after the reaction.

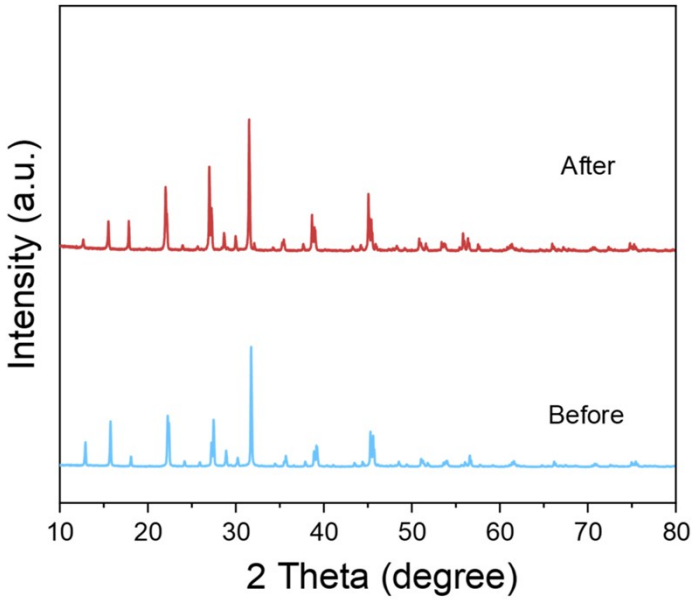

Figure S12. XRD patterns of CsPCN-CBB composite after reaction.

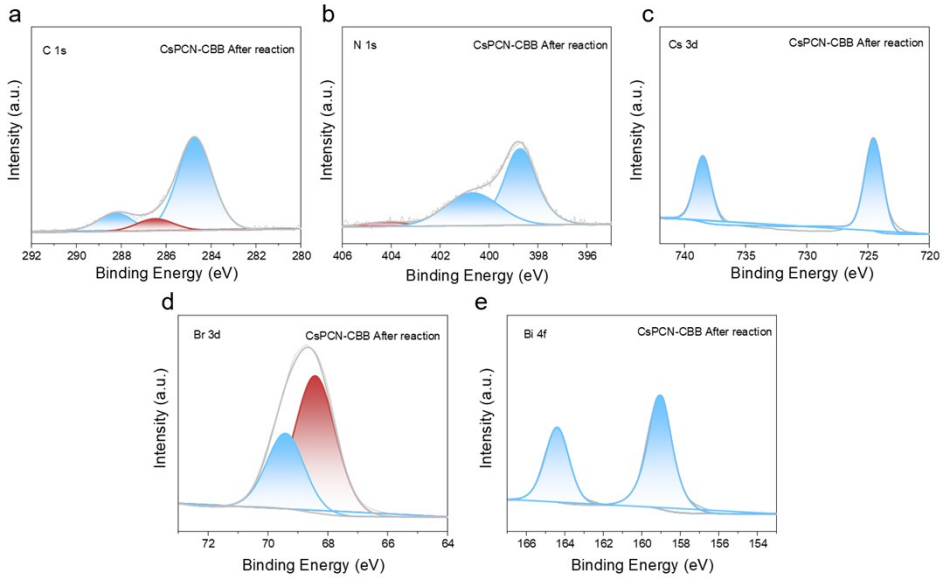

Figure S13. High-resolution XPS spectra of (a) C 1s, (b) N 1s, (c) Cs 3d, (d) Br 3d and (e) Bi 4f of CsPCN-CBB composite after reaction.

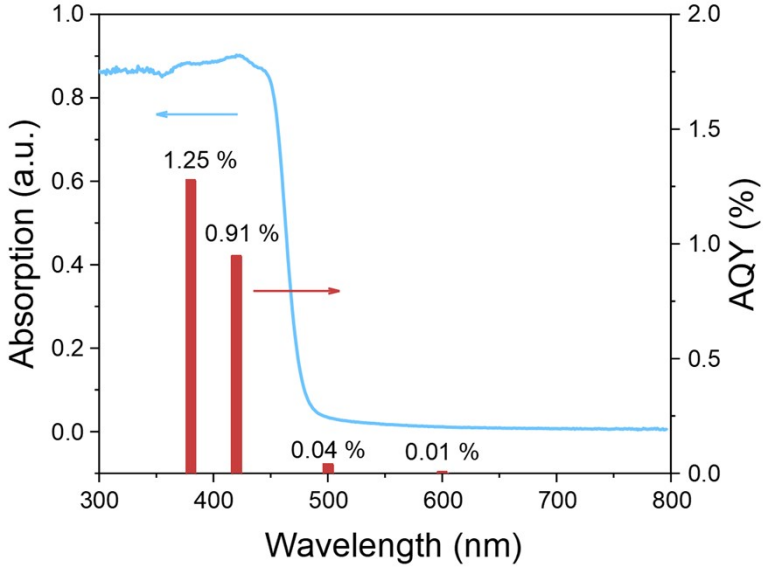

Figure S14. Wavelength-dependent AQY for acetophenone production over CsPCN-CBB.

Note: The apparent quantum yield (AQY) at 420 nm for the conversion of ethylbenzene was measured under the xenon lamp equipped with 420 nm single-wavelength filters over 1 h. The total illustration was 0.023 W cm^{-2}. The irradiation area was controlled as 19.6 cm^2.

Table S1. Photocatalytic activity of different catalysts toward different reaction substrates.

catalyst / Reactant	CsPCN	CBB	CsPCN-CBB
Ethylbenzene	967	1950	8420
Toluene	873	2383	7253
Benzyl alcohol	517	1432	5158
Diphenylmethane	758	2047	6138
Cyclohexane	737	2150	7193
Benzylamine	764	2342	7438

Table S2. Comparison of the photocatalytic aerobic oxidation of ethylbenzene activities of the reported materials.

Catalyst	Oxidant	Substrate	Wavelength/Temperature	Acetophenone production rate ($\mu mol \cdot g^{-1} \cdot h^{-1}$)	Ref.
$BiVO_4/Ag/C_3N_4$	O_2	1 mmol	($\lambda > 400$ nm)	140	[1]
CuW-TPT	O_2	0.5 mmol	365 nm LED light	687.5	[2]
p-BiOBr	O_2	0.2 mmol	($\lambda > 400$ nm)	930	[3]
BiOCl	O_2	0.2 mmol	405 nm LED	866	[4]
Mo-BiOCl	O_2	0.2 mmol	405 nm LED	8033	[4]
Bi_2MoO_6-C	O_2	1.5 mL	($\lambda > 420$ nm)	1100	[5]
4CD/BiMO	O_2	0.35 mmol	($\lambda > 400$ nm)	416	[5]
TCN	O_2	0.5 mmol	($\lambda > 400$ nm)	658.7	[6]
SA-Fe-TCN	O_2	0.5 mmol	($\lambda > 400$ nm)	4083	[6]
P-TTEPY-C6	O_2	0.1 mmol	365 nm LED light	4125	[7]
Bi_2MoO_6	O_2	10 mmol	($\lambda > 400$ nm)	391.2	[8]
TiO_2/Bi_2MoO_6	O_2	10 mmol	($\lambda > 400$ nm)	1036	[8]
MMO-0.5/A	TBHP	10 mmol	120 °C	4656	[9]
Co/CoO@N-HMCS	TBHP	2 mmol	80 °C	5394	[10]
SACo@ g-C_3N_4	PMS	0.1 mmol	60 °C	1242.6	[11]
TTT-COF	O_2	0.1 mmol	($\lambda > 420$ nm)	1225	[12]
C-Nb_2O_5	O_2	20 mmol	Blue LED light (λ=400-405 nm)	1256	[13]
PdO/C-Nb_2O_5	O_2	20 mmol	Blue LED light (λ=400-405 nm)	10997	[13]
h-MoO_3	O_2	3 mL	405 nm LED	20400	[14]
W-TiO_2	O_2	3 mL	437 nm LED	19333	[15]
TiO_2-PEG200	O_2	3 mL	405 nm LED	56000	[16]
CsPCN-CBB	O_2	1 mmol	($\lambda > 420$ nm)	8420	This work
CsPCN-CBB	O_2	1 mmol	420 nm LED	32800	This work

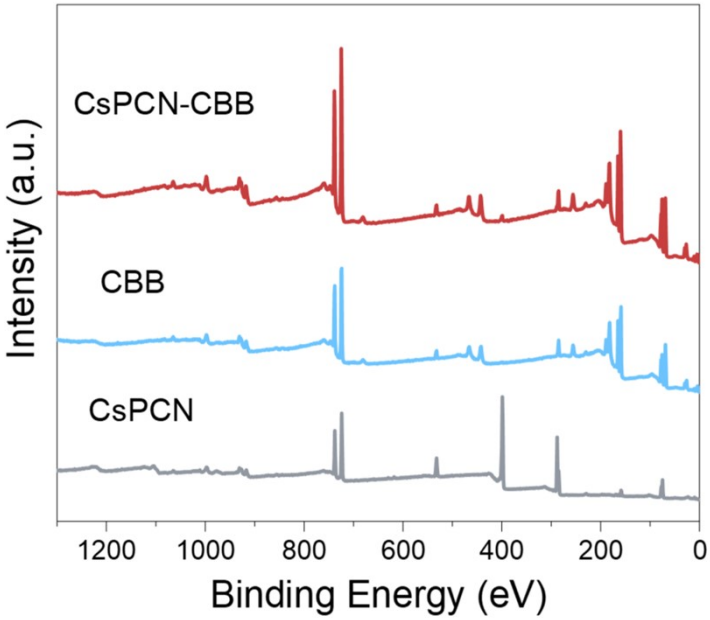

Figure S15. XPS survey spectra of CsPCN, CBB and CsPCN-CBB.

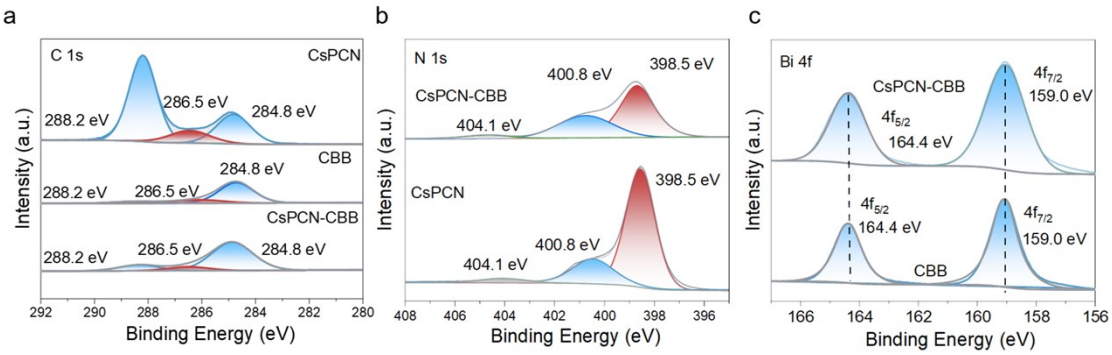

Figure S16. High-resolution XPS spectra of (a) C 1s, (b) N 1s and (c) Bi 4f core levels of CsPCN, CBB and CsPCN-CBB composites.

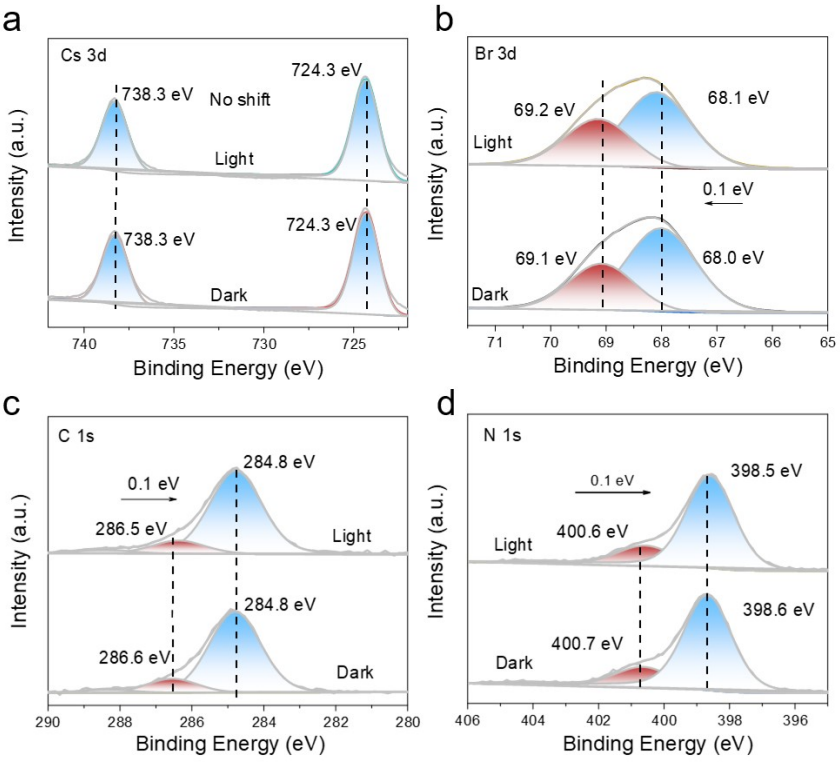

Figure S17. *In-situ* XPS spectra of Cs 3d (a), Br 3d (b), C 1s (c) and N 1s (d) in CsPCN-CBB composites.

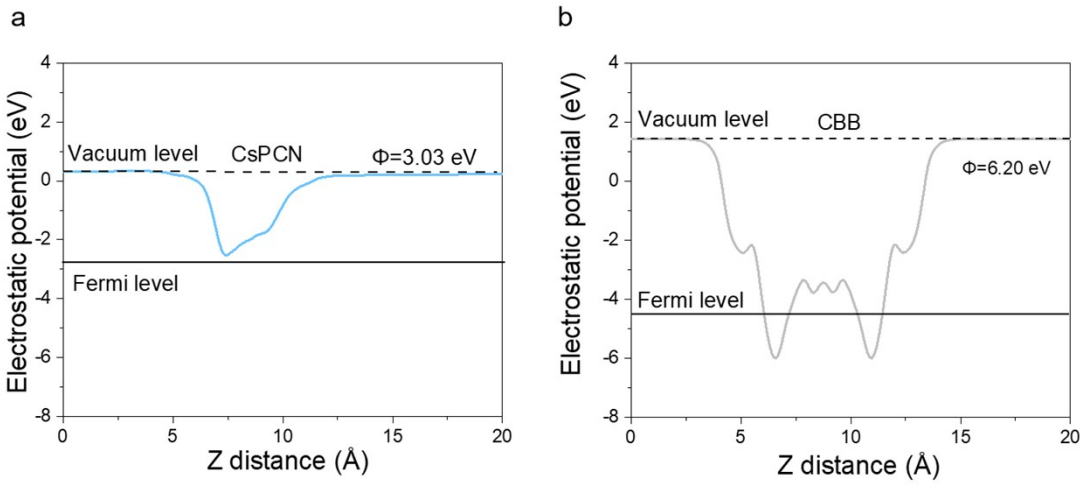

Figure S18. Work functions of (a) CsPCN and (b) CBB.

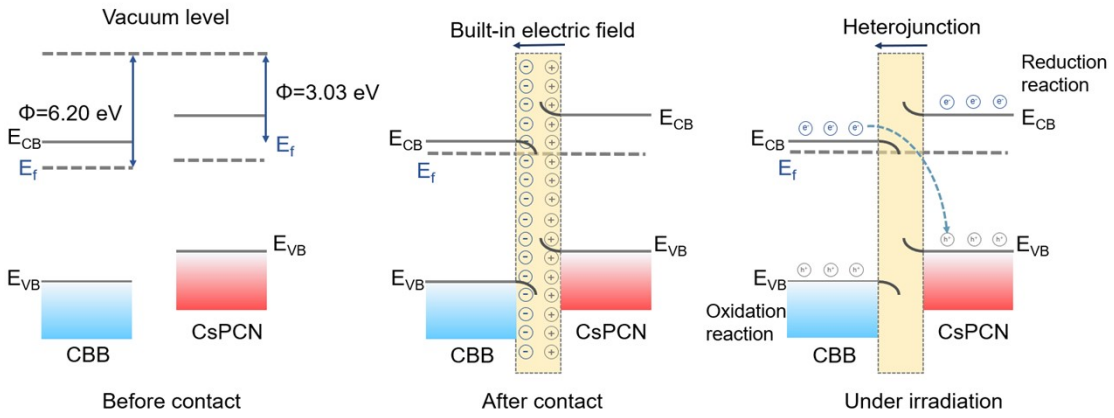

Figure S19. Schematic illustration of band alignments of blank CBB and CsPCN before and after contact, and the charge transfer process of CsPCN-CBB composite under visible light irradiation.

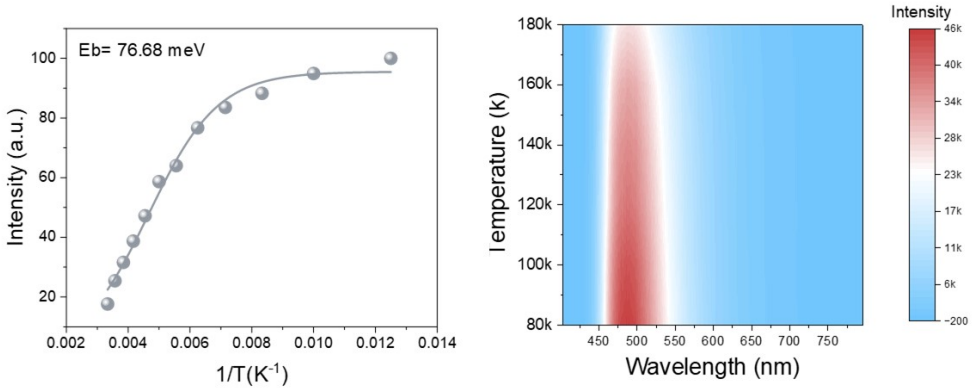

Figure S20. Temperature-dependent photoluminescence of CsPCN.

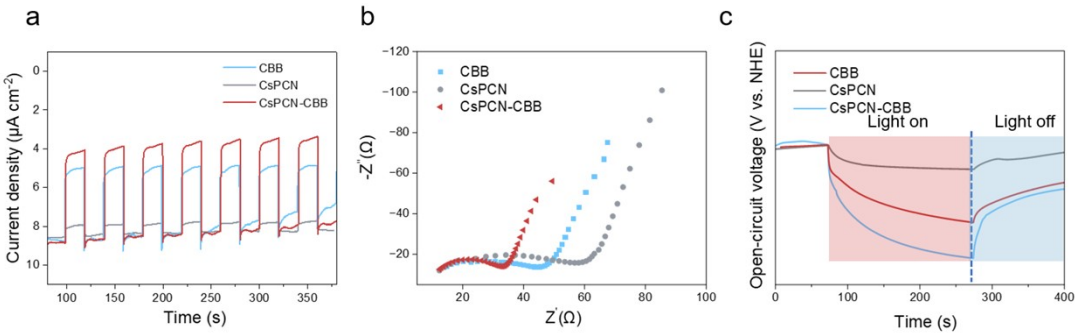

Figure S21. (a) Transient photocurrents (b) EIS spectra and (c) Open-circuit voltage decay (OCVD) of CsPCN, CBB and CsPCN-CBB composites.

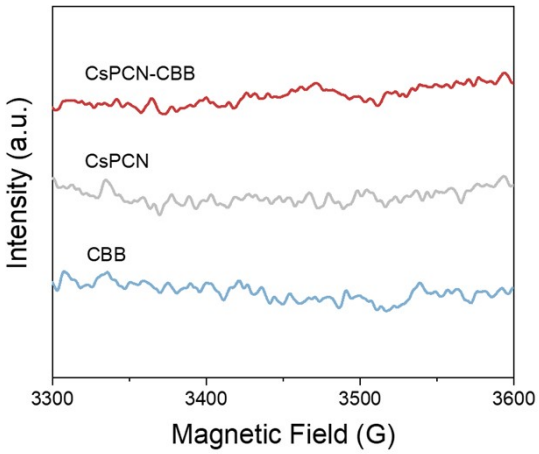

Figure S22. EPR detection of DMPO-$RCHCH_3^{\cdot-}$ over blank CBB, CsPCN and CsPCN-CBB under dark conditions.

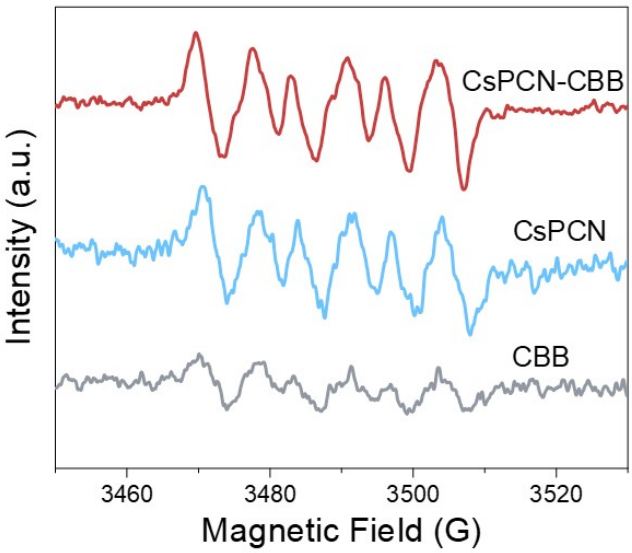

Figure S23. *In-situ* EPR test of CsPCN, CBB and CsPCN-CBB composite in the presence of DMPO with light irradiation.

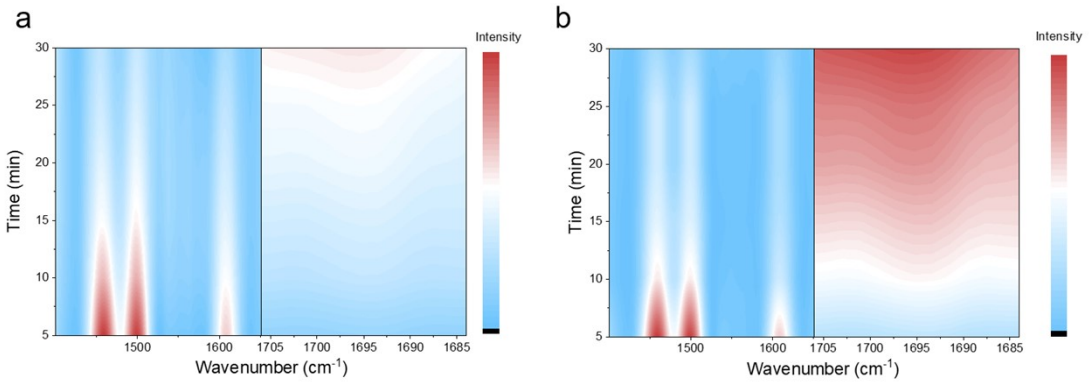

Figure S24. *In-situ* DRIFTS of blank (a) CBB and (b) CsPCN-CBB composite.

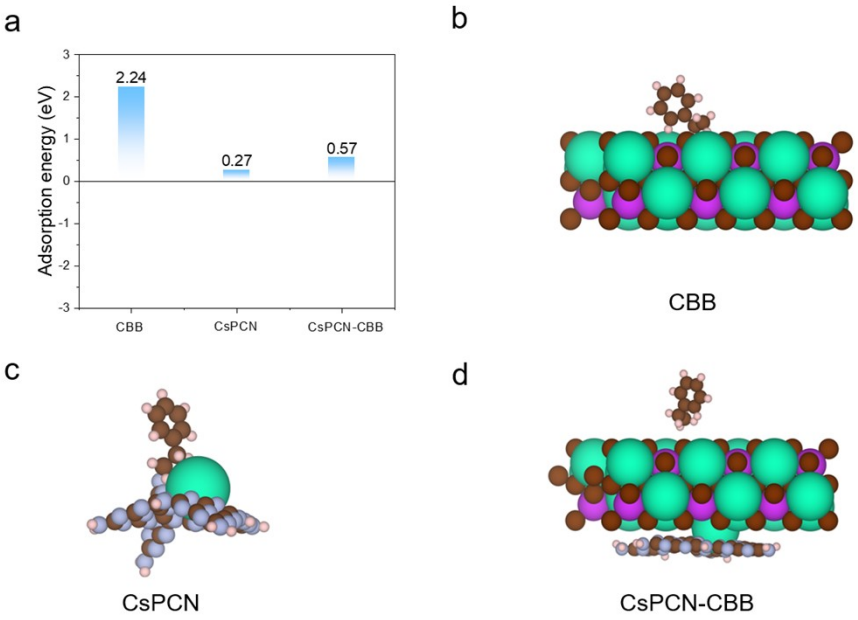

Figure S25. (a) Adsorption energy of ethylbenzene on CBB, CsPCN and CsPCN-CBB, (b-d) adsorption model of different photocatalysts.

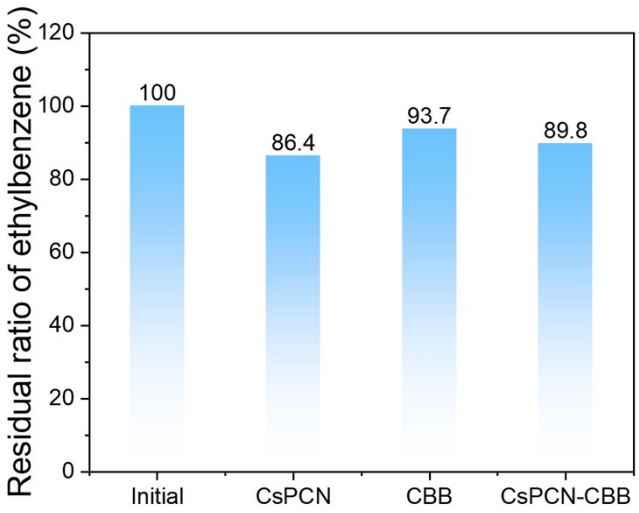

Figure S26. Normalized adsorption experiments of ethylbenzene.

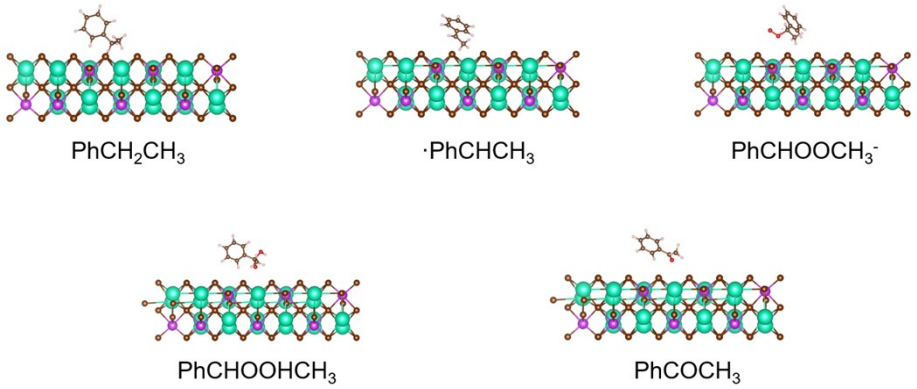

Figure S27. Optimized configurations of CBB.

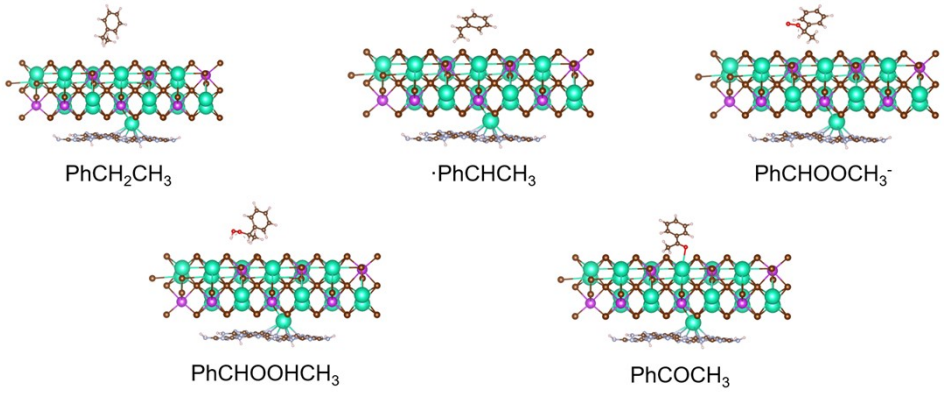

Figure S28. Optimized configurations of CsPCN-CBB.

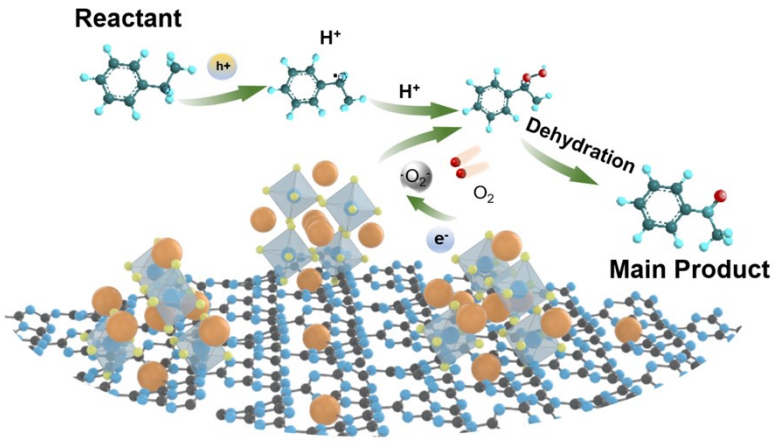

Figure S29. Illustration of the mechanism for photocatalytic ethylbenzene oxidation over CsPCN-CBB composite.

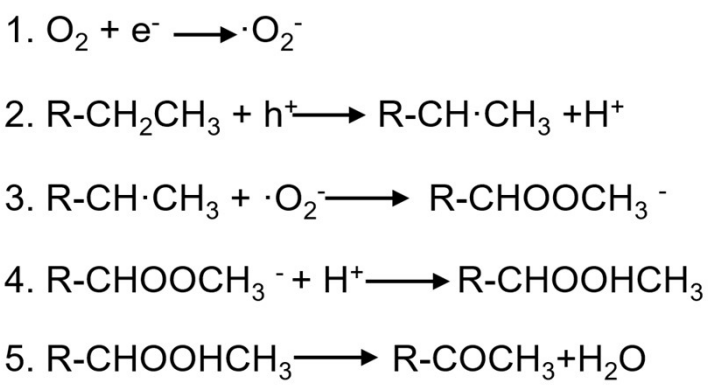

Figure S30. The chemical reaction equations for photocatalytic ethylbenzene oxidation under light irradiation.

Reference:

1 P. Chen, Y. Li, C. Xiao, L. Chen, J.-K. Guo, S. Shen, C.-T. Au and S.-F. Yin, *ACS Sustainable Chem. Eng.* 2019, **7**, 17500-17506.

2 J. Jiao, T. Zhang, J. Xu, K. Guo, J. Li and Q. Han, *Chem. Commun.* 2023, **59**, 3114-3117.

3 X. Cao, A. Huang, C. Liang, H.-C. Chen, T. Han, R. Lin, Q. Peng, Z. Zhuang, R. Shen, H. M. Chen, Y. Yu, C. Chen and Y. Li, *J. Am. Chem. Soc.* 2022, **144**, 3386-3397.

4 D. Kong, G. Ji, Y. Dou, M. Yan, Y. Zhang and W. Wang, *J. Catal.* 2025, **443**, 115987.

5 X. Yang, X. Li, B. Zhang, T. Liu and Z. Chen, *ACS Sustainable Chem. Eng.* 2024, **12**, 6519-6528.

6 X. Xiao, Z. Ruan, Q. Li, L. Zhang, H. Meng, Q. Zhang, H. Bao, B. Jiang, J. Zhou, C. Guo, X. Wang and H. Fu, *Adv. Mater.* 2022, **34**, 2200612.

7 S. Ma, Q. Liu, J. Cui, C. Rao, M. Jia, X. Yao and J. Zhang, *J. Colloid Interf. Sci.* 2023, **634**, 431-439.

8 L.-N. Song, F. Ding, Y.-K. Yang, D. Ding, L. Chen, C.-T. Au and S.-F. Yin, *ACS Sustainable Chem. Eng.* 2018, **6**, 17044-17050.

9 R. Xie, G. Fan, L. Yang and F. Li, *Catal. Sci. Technol.* 2015, **5**, 540-548.

10 C. Yi, J. Huo and Z. Liu, *Chem. Eng. J.* 2023, **467**, 143541.

11 J. Li, S. Zhao, S.-Z. Yang, S. Wang, H. Sun, S. P. Jiang, B. Johannessen and S. Liu, *J. Mater. Chem. A* 2021, **9**, 3029-3035.

12 J. Yang, Z. Zhao, X. Liu, H. Yang, J. Yang, M. Zhou, S. Li, X. Liu, X. Xu and C. Cheng, *Nat. Commun.* 2025, **16**, 7654.

13 X. Jiang, W. Wang, H. Wang, Z.-H. He, Y. Yang, K. Wang, Z.-T. Liu and B. Han, *Green Chem.* 2024, **26**, 4552-4562.

14 Y. Qin, G. Ji, Y. Zhang, M. Yan, Y. Dou and W. Wang, *Chem. Eng. J.* 2025, **507**, 160562.

15 Z. Zhang, Y. Zhang, C. Han, M. Yan, G. Ji and W. Wang, *Inorg. Chem. Front.* 2025, **12**, 4720-4730.

16 Y. Zhang, D. Kong, X. Li, G. Ji, F. Liu, Y. Dou and W. Wang, *Chem. Eng. J.* 2025, **524**, 169805.